

Learning-based data-enabled moving horizon estimation with application to membrane-based biological wastewater treatment process ^{*}

Xiaojie Li ^{*} Xunyuan Yin ^{*,**,1}

^{*} School of Chemistry, Chemical Engineering and Biotechnology, Nanyang Technological University, 62 Nanyang Drive, 637459, Singapore (e-mail: xiaojie002@e.ntu.edu.sg, xunyuan.yin@ntu.edu.sg)
^{**} Nanyang Environment and Water Research Institute, Nanyang Technological University, 1 CleanTech Loop, 637141, Singapore

Abstract: In this paper, we propose a data-enabled moving horizon estimation (MHE) approach for nonlinear systems. While the approach is formulated by leveraging Koopman theory, its implementation does not require explicit Koopman modeling. Lifting functions are learned from the state and input data of the original nonlinear system to project the system trajectories into the lifted space, where the resulting trajectories implicitly describe the Koopman representation for the original nonlinear system. A convex data-enabled MHE formulation is developed to provide real-time state estimates of the Koopman representation, from which the states of the nonlinear system can be reconstructed. Sufficient conditions are derived to ensure the stability of the estimation error. The effectiveness of the proposed method is illustrated using a membrane-based biological water treatment process.

Keywords: Data-enabled state estimation, moving horizon estimation, nonlinear system, membrane bioreactor process

1. INTRODUCTION

Full-state information is critical for implementing various advanced control designs (Allgöwer and Zheng (2012), Lee and Lee (2014)). However, for complex nonlinear systems, obtaining such information in real time is often difficult or prohibitively expensive (Bourgeois et al. (2001), Turan and Ferrari-Trecate (2021)). Nonlinear state estimation offers a practical alternative by reconstructing the full states from limited output measurements (Kottakki et al. (2014), Shao et al. (2010)). Among available approaches, moving horizon estimation (MHE) is one of the well-suited frameworks to nonlinear processes, since it can explicitly handle constraints and nonlinearity by incorporating them into an online optimization problem (Rao et al. (2003)).

MHE performance typically depends on the accuracy of the system dynamic model. When first-principles models are accessible or when data-driven models are obtained through system identification, MHE can be formulated based on such models (Rao et al. (2001), Rao et al. (2003), Yin et al. (2023)). A promising alternative is to develop data-enabled MHE schemes that bypass explicit model identification and directly construct the estimator from data (Wolff et al. (2024)). Willems' fundamental lemma (Willems et al. (2005)), which enables implicit

representation of a linear time-invariant (LTI) system using its trajectories, has emerged as a powerful foundation for direct data-enabled control (Berberich and Allgöwer (2020), Morato and Felix (2024)) and direct data-enabled state estimation (Wolff et al. (2024), Turan and Ferrari-Trecate (2021)).

Willems' fundamental lemma (Willems et al. (2005)) has been leveraged for state estimation. Within this direct data-enabled framework, a Luenberger observer was developed in Adachi and Wakasa (2021). To address the unknown inputs or disturbances, an unknown input observer integrating Willems' fundamental lemma was proposed in Turan and Ferrari-Trecate (2021). A data-enabled MHE approach capable of handling state constraints was proposed in Wolff et al. (2024) to achieve robustness against measurement noise in offline data. However, it is worth mentioning that the theoretical results of the above-mentioned data-enabled state estimation approaches are limited to linear systems, since Willems' fundamental lemma is solely applicable to LTI systems.

In this work, we propose a data-enabled MHE approach for general nonlinear systems. The proposed method utilizes a linear parameter-varying (LPV) Koopman representation to facilitate state estimator design. Explicit Koopman modeling is not required; instead, neural networks are employed to generate its trajectories directly from system data. Subsequently, a data-enabled MHE is formulated in the lifted space using the trajectories of the Koopman surrogate. The proposed MHE scheme estimates the states of

^{*} This research is supported by Ministry of Education, Singapore, under its Academic Research Fund Tier 1 (RG95/24 & RG63/22).

¹ Corresponding author: Xunyuan Yin. Tel: (+65) 6316 8746. Email: xunyuan.yin@ntu.edu.sg

the Koopman surrogate, based on which the original states of the nonlinear system are reconstructed. Additionally, we establish the stability of the proposed data-enabled MHE method and demonstrate its effectiveness and superiority through a simulated application to a membrane-based bioreactor process used for wastewater treatment.

2. PRELIMINARIES

2.1 Notation

\mathbb{N} represents the set of non-negative integers. $\mathbb{N}_{[a,b]} := \mathbb{N} \cap [a, b]$ denotes the set of non-negative integers within the interval $[a, b]$. Q^\dagger denotes the Moore-Penrose pseudoinverse of matrix Q . For a vector z , $\|z\|$ is the Euclidean norm; $\|z\|_Q^2 := z^\top Q z$ denotes the square of weighted Euclidean norm; $\|z\|_\infty := \max_i |z_i|$ represents the infinity norm. Given a sequence $\{z_j\}_a^b$, the stacked vector $z_{[a,b]}$ is defined as $z_{[a,b]} := [z_a^\top, \dots, z_b^\top]^\top$. \otimes denotes the Kronecker product. \mathbb{E} represents the expectation. Let $\mathbb{R}_+ := [0, \infty)$, a function $\kappa : \mathbb{R}_+ \rightarrow \mathbb{R}_+$ belongs to class \mathcal{K} if it is continuous, strictly increasing, and satisfies $\kappa(0) = 0$. The Hankel matrix of depth N associated with $z_{[a,b]}$ is defined as

$$\mathcal{H}_N(z_{[a,b]}) := \begin{bmatrix} z_a & z_{a+1} & \dots & z_{b-N+1} \\ z_{a+1} & z_{a+2} & \dots & z_{b-N+2} \\ \vdots & \vdots & \ddots & \vdots \\ z_{a+N-1} & z_{a+N} & \dots & z_b \end{bmatrix}$$

2.2 System description

We consider a class of discrete-time nonlinear systems of the following form:

$$x_{k+1} = f(x_k, u_k), \quad y_k = Cx_k \quad (1)$$

where $x_k \in \mathcal{X} \subseteq \mathbb{R}^{n_x}$ is the vector of system states; $u_k \in \mathcal{U} \subseteq \mathbb{R}^{n_u}$ is the vector of known inputs; $y_k \in \mathbb{R}^{n_y}$ denotes the vector of measured outputs; $f : \mathcal{X} \times \mathcal{U} \rightarrow \mathcal{X}$ is a continuous, nonlinear function characterizing the dynamics of system (1); $C \in \mathbb{R}^{n_y \times n_x}$ is the output matrix; \mathcal{X} and \mathcal{U} are compact convex sets.

The nonlinear function f and output matrix C of system (1) are unknown. Instead, only data trajectories of the system in (1) are available. We consider a two-stage state estimation in the data-enabled framework, which consists of an offline stage for data collection and an online stage for real-time state estimation (Wolff et al. (2024)). Specifically, in the offline stage, trajectories of noise-free inputs $\{u_k^o\}_0^{T-1}$, noisy states $\{\tilde{x}_k^o\}_0^T$, and noisy measured outputs $\{\tilde{y}_k^o\}_0^T$ are collected. We consider that the state and output measurements are contaminated by unknown but bounded measurement noise (Wolff et al. (2024)):

$$\tilde{x}_k^o = x_k^o + \varepsilon_{x,k}^o, \quad \tilde{y}_k^o = y_k^o + \varepsilon_{y,k}^o$$

where x_k^o and y_k^o are noise-free states and measured outputs of system (1), respectively; $\varepsilon_{x,k}^o$ and $\varepsilon_{y,k}^o$ are bounded state and output measurement noise, respectively, satisfying $\|\varepsilon_{x,k}^o\|_\infty \leq \bar{\varepsilon}_x$ and $\|\varepsilon_{y,k}^o\|_\infty \leq \bar{\varepsilon}_y$, $\forall k \in \mathbb{N}$. Throughout this paper, the superscript o indicates that the corresponding data are collected in the offline stage. In the online stage, system states are no longer measurable and need to be estimated using available input and output data.

Remark 1. Although full-state measurements are not accessible during online implementation, they can be obtained using lab analyzers or high-fidelity sensors. For example, in chemical and biological processes, substance concentrations can be obtained by laboratory analyzers (Bourgeois et al. (2001), Nicoletti et al. (2009)). In autonomous driving, the full state of vehicles can be measured through high-fidelity sensors during the off-line/testing phases (Turan and Ferrari-Trecate (2021), Wolff et al. (2024)).

2.3 LPV Koopman representation of controlled systems

Koopman operator theory (Koopman (1931)) is originally developed for autonomous systems, which provides a promising framework for describing dynamics of nonlinear systems using a linear representation by lifting the original system states into a higher-dimensional space. For nonlinear controlled systems in (1), an exact Koopman representation has the following form (Iacob et al. (2024)):

$$z_{k+1} = Az_k + \phi(x_k, u_k)u_k \quad (2)$$

where $z_k = \psi(x_k) \in \mathbb{R}^{n_z}$ denotes the state vector in the lifted space; $\psi : \mathcal{X} \rightarrow \mathbb{R}^{n_z}$ is the state lifting function; $\phi : \mathcal{X} \times \mathcal{U} \rightarrow \mathbb{R}^{n_z \times n_u}$ describes the input matrix in the lifted space. Based on the factorization method proposed in Iacob et al. (2024), the Koopman model in (2) can be rewritten in a linear parameter-varying (LPV) form:

$$z_{k+1} = Az_k + \beta(p_k)u_k \quad (3)$$

where $p_k = \lambda(z_k, u_k) \in \mathbb{R}^{n_p}$ is the scheduling parameter with scheduling map $\lambda : \mathbb{R}^{n_z} \times \mathcal{U} \rightarrow \mathbb{R}^{n_p}$; $\beta : \mathbb{R}^{n_p} \rightarrow \mathbb{R}^{n_z \times n_u}$ is the input matrix satisfying $\beta \circ \lambda = \phi$.

2.4 Problem formulation

The objective of this paper is to develop a data-enabled state estimation method that can provide real-time state estimates for nonlinear systems in (1), without explicitly constructing a dynamic model. Specifically, we first leverage the Koopman modeling method in Iacob et al. (2024) to derive a Koopman-based LPV representation for the nonlinear systems (1) in a lifted state space. Note that the explicit identification of this Koopman-based LPV representation is not required. Instead, we focus on constructing trajectories of this Koopman-based representation using the trajectories of nonlinear system (1). Based on the constructed trajectories, we aim to formulate a convex optimization-based, data-enabled state estimation method to provide real-time estimates of the states in the Koopman-based representation, from which the states of nonlinear system (1) can be reconstructed.

3. TRAJECTORY-BASED REPRESENTATION OF SURROGATE

In this work, we consider $\beta(p_k)$ in (3) to have affine dependence on p_k (Tóth et al. (2011)):

$$\beta(p_k) = B_0 + \sum_{i=1}^{n_p} p_{k,i} B_i \quad (4)$$

where $p_{k,i}$ denotes the i th element of p_k and $B_i \in \mathbb{R}^{n_z \times n_u}$ for $i \in \mathbb{N}_{[1, n_p]}$. By denoting $\tilde{B} = [B_1, \dots, B_{n_p}]$, the LPV representation in (3) can be reformulated as

$$z_{k+1} = Az_k + B_0 u_k + \tilde{B}(p_k \otimes u_k) \quad (5)$$

Before proceeding further, we define $B = [B_0, \tilde{B}]$ and $v_k := p_k \otimes u_k$.

Definition 1. (Willems et al. (2005)) $\{u_k\}_0^{T-1}$ is persistently exciting of order N , if $\text{rank}(\mathcal{H}_N(u_{[0,T-1]})) = Nn_u$.

Assumption 1. The pair (A, B) is controllable and the offline augmented input sequence $\{[(u_k^o)^\top, (v_k^o)^\top]^\top\}_0^{T-1}$ is persistently exciting of order $N + n_z + 1$.

Assumption 2. There exists an exact LPV Koopman representation (5) for nonlinear system (1).

Assumption 3. There exists a reconstruction matrix $D \in \mathbb{R}^{n_x \times n_z}$ for (5), such that it holds for all $k \in \mathbb{N}$ that:

$$x_k = D\psi(x_k) \quad (6)$$

Following Xiong et al. (2025), Assumption 2 requires the existence of an exact Koopman representation of (1). Based on Iacob et al. (2025), Assumption 3 requires that states x_k of (1) can be reconstructed from states $z_k = \psi(x_k)$ of Koopman representation (5). Note that Assumptions 2-3 are only utilized in Theorem 1 to establish an implicit representation of (5); these assumptions are not required for the stability analysis in Theorem 2. Under Assumptions 2-3, it follows from (1) and (6) that

$$y_k = CD\psi(x_k) \quad (7)$$

In the following, we consider the Koopman surrogate consisting of (5) and (7), which has the same inputs and outputs as the original nonlinear system (1).

Theorem 1. Consider an input/output/state trajectory $\{u_k^o, y_k^o, x_k^o\}_0^{T-1}$ of nonlinear system (1) and a scheduling parameter trajectory $\{p_k^o\}_0^{T-1}$ of its corresponding LPV Koopman surrogate consisting of (5) and (7). If Assumptions 1-3 hold, then the following holds:

- (i) $\text{rank} \begin{pmatrix} \mathcal{H}_1(\psi(x^o)_{[0,T-1]}) \\ \mathcal{H}_N(u_{[0,T-1]}^o) \\ \mathcal{H}_N(v_{[0,T-1]}^o) \end{pmatrix} = n_z + Nn_u(1 + n_p)$
- (ii) $\{u_k, y_k, p_k\}_0^{N-1}$ is an input/output/parameter trajectory of (5) and (7), if and only if there exists $\alpha \in \mathbb{R}^{T-N+1}$ such that

$$\begin{bmatrix} \mathcal{H}_N(u_{[0,T-1]}^o) \\ \mathcal{H}_N(v_{[0,T-1]}^o) \\ \mathcal{H}_N(y_{[0,T-1]}^o) \end{bmatrix} \alpha = \begin{bmatrix} u_{[0,N-1]} \\ v_{[0,N-1]} \\ y_{[0,N-1]} \end{bmatrix} \quad (8)$$

Proof. By defining an augmented input vector $\mathbf{u}_k = [u_k^\top, v_k^\top]^\top$, (5) can be reformulated in the linear time-invariant form:

$$z_{k+1} = Az_k + B\mathbf{u}_k \quad (9)$$

Based on (9), both (i) and (ii) can be established following the proof of Theorem 1 in Van Waarde et al. (2020). \square

According to Berberich and Allgöwer (2020), the following relationship holds:

$$\mathcal{H}_N(\psi(x^o)_{[0,T-1]})\alpha = \psi(x)_{[0,N-1]} \quad (10)$$

It is worth noting that the outputs of the Koopman surrogate are not required to be identical to those of the original nonlinear system (1). Instead, any output that is linear with respect to the state of (5) can be selected to construct an implicit representation for (5). By selecting (6) as the measurement model for (5), it holds that

$$\mathcal{H}_N(x_{[0,T-1]}^o)\alpha = x_{[0,N-1]} \quad (11)$$

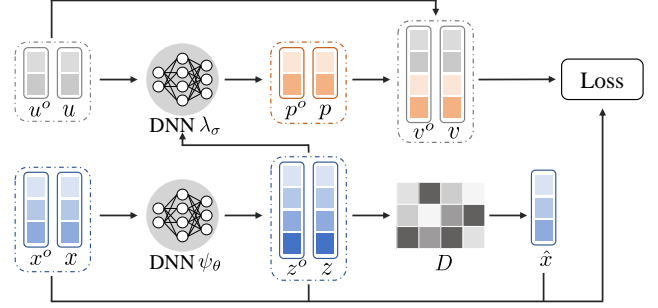


Fig. 1. An illustrative diagram of the proposed data-enabled MHE.

4. LEARNING-BASED DATA-ENABLED MOVING HORIZON ESTIMATION

4.1 Training process

According to Theorem 1, it is sufficient to describe (5) using its input, output, state, and parameter trajectories without the need to identify an explicit representation. In this section, we treat x_k as the output of Koopman surrogate since full-state information can be obtained during the offline stage as discussed in Remark 1. Therefore, (6) is adopted as the measurement model for the Koopman surrogate. Specifically, the input u_k and output x_k of Koopman surrogate (5)-(6) can be directly obtained from (1), while its state z_k and the scheduling parameter p_k are not directly measurable. Note that both z_k and p_k can be determined from x_k and u_k , if the lifting function ψ and the scheduling mapping λ are known. Therefore, the objective of this section is to approximate functions ψ and λ using two dense neural networks (DNNs) (Rumelhart et al. (1986)), which can generate z_k and p_k directly from the data of nonlinear system (1).

A training dataset \mathcal{D} consists of two open-loop input and state trajectories: 1) $\{u_k^o\}_0^{T-1}$ and $\{x_k^o\}_0^T$ used to construct the Hankel matrices; 2) $\{u_k\}_0^{N-1}$ and $\{\tilde{x}_k\}_0^N$ used for online prediction. Fig. 1 shows an illustrative diagram of the training process of the proposed learning-based data-enabled MHE. Specifically, the trained neural network ψ_θ projects the original state x_k to a higher-dimensional space to obtain the state z_k for (5) as follows:

$$z_k = \psi_\theta(x_k|\theta) \quad (12)$$

where θ denotes the trainable parameters of neural network ψ_θ . Given the input u_k and state z_k of (5), the neural network λ_σ is utilized to approximate the scheduling parameter p_k for Koopman surrogate (5)-(6). The structure of λ_σ is designed as follows:

$$p_k = \lambda_\sigma(z_k, u_k|\sigma) \quad (13)$$

where σ includes the trainable parameters of neural network λ_σ . Moreover, the reconstruction matrix D , which reconstructs the original system state x_k from the lifted state z_k , is also treated as part of the trainable parameters.

The optimization problem associated with offline training is formulated as follows:

$$\min_{\theta, \sigma, D} \mathcal{L} = \mathcal{L}_1 + \mathcal{L}_2 \quad (14)$$

where \mathcal{L}_1 and \mathcal{L}_2 are defined as follows:

$$\mathcal{L}_1 = \mathbb{E}_D \sum_{i=0}^N \|Dz_i - x_i\|$$

$$\mathcal{L}_2 = \mathbb{E}_D \left\| D\mathcal{H}_{N+1}(z_{[0,T]}^o) \begin{bmatrix} \mathcal{H}_N(u_{[0,T-1]}^o) \\ \mathcal{H}_N(v_{[0,T-1]}^o) \\ \mathcal{H}_{N+1}(x_{[0,T]}^o) \end{bmatrix}^\dagger \begin{bmatrix} u_{[0,N-1]} \\ v_{[0,N-1]} \\ x_{[0,N]} \end{bmatrix} - x_{[0,N]} \right\|$$

The loss term \mathcal{L}_1 penalizes the error between the states reconstructed by matrix D and the actual states, while \mathcal{L}_2 penalizes the discrepancy between the states predicted by the implicit representation of Koopman surrogate (5)-(6) and the actual states of the nonlinear system (1).

4.2 Data-enabled MHE in lifted space

In practice, modeling residuals inevitably arise from the LPV approximation in (4) and/or from the neural network-based approximations of the lifting function ψ_θ and scheduling mapping λ_σ . To account for these modeling residuals, we suppose that an exact LPV Koopman surrogate can be expressed in the following form:

$$z_{k+1} = Az_k + B_0 u_k + \tilde{B}(p_k \otimes u_k) + w_k \quad (15a)$$

$$y_k = CDz_k + d_k \quad (15b)$$

$$x_k = Dz_k + r_k \quad (15c)$$

where w_k , d_k , and r_k represent unknown modeling residuals. The lifted state, measured output, and reconstructed state of the nominal version of (15), which includes (5), (6), and (7), are denoted by z'_k , y'_k , and x'_k , respectively.

Assumption 4. The scheduling mapping λ_σ is continuous, and lifting function ψ_θ is locally Lipschitz continuous on \mathcal{X} , which satisfies $\|\psi_\theta(x) - \psi_\theta(\check{x})\| \leq L_\psi \|x - \check{x}\|, \forall x, \check{x} \in \mathcal{X}$.

Proposition 1. If Assumption 4 holds, there exist bounds \bar{w} , \bar{d} , \bar{r} , such that $\|w_k\|_\infty \leq \bar{w}$, $\|d_k\|_\infty \leq \bar{d}$, and $\|r_k\|_\infty \leq \bar{r}$ hold for all $k \in \mathbb{N}$.

Proof. This proposition can be proven following the proof of Proposition 2 in Zhang et al. (2022).

During the offline stage, we consider (15) and its nominal version are initialized with the same initial condition $z_0^o = z_0^o$, and evolve under the same input sequence $\mathbf{u}^o := \{u_k^o\}_{0}^{T-1}$ and scheduling parameter sequence $\mathbf{p}^o := \{p_k^o\}_{0}^{T-1}$. State and output deviations at time instant k are given by $\Delta z_k^o := z_k^o - z_k^o = \sum_{i=0}^{k-1} A^{k-1-i} w_i^o$ and $\Delta y_k^o := y_k^o - y_k^o = CD\Delta z_k^o + d_k^o$. From Proposition 1, there exist bounds $\bar{\Delta}_z^o := \sum_{i=0}^{T-1} \|A\|^{k-1-i} \bar{w}$ and $\bar{\Delta}_y^o = \|C\| \|D\| \bar{\Delta}_z^o + \bar{d}$ such that $\|\Delta z_k^o\| \leq \bar{\Delta}_z^o$ and $\|\Delta y_k^o\| \leq \bar{\Delta}_y^o, \forall k \in \mathbb{N}_{[0,T]}$.

For online implementation, (7) is adopted as the measurement model for (5) since the state trajectory is not directly accessible. According to Theorem 1, the input, output, state, and parameter trajectories of the Koopman surrogate in (5) and (7) serve as an implicit representation, based on which, a data-enabled MHE approach is developed in the lifted space. Specifically, at each time instant $k \geq N$, the estimator provides state estimates by solving the following optimization problem:

$$\min_{\hat{z}_{[k-N,k]}, \pi_{[k-N,k]}^y, \pi_{[k-N,k]}^z, \alpha_k} V_k$$

$$\text{s.t. } \begin{bmatrix} \mathcal{H}_N(u_{[0,T-1]}^o) \\ \mathcal{H}_N(v_{[0,T-1]}^o) \\ \mathcal{H}_{N+1}(\hat{y}_{[0,T]}^o) \\ \mathcal{H}_{N+1}(\hat{z}_{[0,T]}^o) \end{bmatrix} \alpha_k = \begin{bmatrix} u_{[k-N,k-1]} \\ v_{[k-N,k-1]} \\ \tilde{y}_{[k-N,k]} - \pi_{[k-N,k]}^y \\ \hat{z}_{[k-N,k]} + \pi_{[k-N,k]}^z \end{bmatrix} \quad (16a)$$

$$D\hat{z}_{j|k} \in \mathcal{X}, j \in \mathbb{N}_{[k-N,k]} \quad (16b)$$

with

$$V_k = \lambda_z \|\hat{z}_{k-N|k} - \bar{z}_{k-N}\|_P^2 + \sum_{j=k-N}^k \|\pi_{j|k}^z\|_Q^2 \quad (16c)$$

$$+ \sum_{j=k-N}^k \|\pi_{j|k}^y\|_R^2 + \lambda_\alpha (\bar{\varepsilon}_x^o + \bar{\varepsilon}_y^o + \bar{\Delta}_z^o + \bar{\Delta}_y^o) \|\alpha_k\|^2$$

where $\hat{z}_{j|k}$ denotes the state estimate of (5) for time instant j , computed at time instant k ; $\pi_{[k-N,k]}^y$ is a sequence of fitting errors that account for the effect of offline/online measurement noise on measured outputs and the modeling residual $d_{[k-N,k]}$; $\pi_{[k-N,k]}^z$ is a sequence of slack variables that account for the noise in the state trajectory $\hat{z}_{[0,T]}^o$ and the modeling residual $w_{[k-N,k]}$; $u_{[k-N,k-1]}$ contains the online noise-free known inputs from time instant $k-N$ to $k-1$; $p_j = \lambda_\sigma(\hat{z}_{j|j}, u_j)$ is the approximated scheduling parameter at time instant j ; $v_j = p_j \otimes u_j$; $\tilde{y}_{[k-N,k]}$ contains the noisy online measured outputs from time instant $k-N$ to k ; $\bar{z}_{k-N} = \hat{z}_{k-N|k-N}$ is the prior estimate of z_{k-N} ; P , Q , and R are positive-definite weighting matrices; λ_z , $\lambda_\alpha > 0$ are tuning parameters. Note that when $k < N$, the data-enabled MHE in (16) reduces to a full-information estimator, obtained by replacing N with k in (16).

Based on (16), the state estimate $\hat{x}_{k|k}$ of system (1) is obtained as $\hat{x}_{k|k} = D\hat{z}_{k|k}$.

4.3 Stability analysis

Let $z(k; z_0, \mathbf{w})$ denote the solution to (15a) at time instant k , given the initial state z_0 , the input sequence $\mathbf{u} := \{u_0, u_1, \dots\}$, the scheduling parameter sequence $\mathbf{p} := \{p_0, p_1, \dots\}$, and modeling residual sequence $\mathbf{w} := \{w_0, w_1, \dots\}$. We omit \mathbf{u} and \mathbf{p} from the notation $z(k; z_0, \mathbf{w})$ for simplicity. Affected by the modeling residual $\mathbf{d} := \{d_0, d_1, \dots\}$, the corresponding measured output of (15b) at time instant k is given by $h(z(k; z_0, \mathbf{w}), \mathbf{d})$.

Definition 2. (i-UEIOSS) (Alessandri (2025)) System (15a)-(15b) is i-UEIOSS if there exist $c_z, c_w, c_h > 0$ and $\xi \in (0, 1)$ such that, for any two solutions $z(k; z_0, \mathbf{w})$ and $z(k; \check{z}_0, \check{\mathbf{w}})$, it holds for all $k \in \mathbb{N}$ that:

$$\begin{aligned} & \|z(k; z_0, \mathbf{w}) - z(k; \check{z}_0, \check{\mathbf{w}})\| \\ & \leq c_z \|z_0 - \check{z}_0\| \xi^k + c_w \sum_{\tau=0}^{k-1} \|w_\tau - \check{w}_\tau\| \xi^{k-1-\tau} \\ & + c_h \sum_{\tau=0}^{k-1} \|h(z(\tau; z_0, \mathbf{w}), \mathbf{d}) - h(z(\tau; \check{z}_0, \check{\mathbf{w}}), \check{\mathbf{d}})\| \xi^{k-1-\tau} \end{aligned} \quad (17)$$

Note that the i-UEIOSS in Alessandri (2025) is formulated in terms of squared norms.

Assumption 5. The pair (A, CD) is detectable.

Assumption 5 indicates the incremental uniform exponential input/output-to-state stability (i-UEIOSS) of system (15a)-(15b).

Theorem 2. Consider system (1) subject to offline measurement noise (i.e., $\varepsilon_{x,k}^o$ and $\varepsilon_{y,k}^o$), online measurement noise $\varepsilon_{y,k}$, and modeling residuals (i.e., w_k , d_k , r_k) with respect to its corresponding Koopman surrogate (15). If Assumptions 1, 4, and 5 hold and if the parameters of the MHE design (16) are properly tuned, then there exist γ_z , γ_w , γ_ε , $\gamma_d > 0$, $\theta_z \in (0, 1)$, and $\theta \in \mathcal{K}$, such that the following condition holds for all $k \in \mathbb{N}$:

$$\|x_k - \hat{x}_{k|k}^*\| \leq \gamma_z \|x_0 - \bar{x}_0\| \theta_z^k + \theta(\delta) \quad (18)$$

$$+ \gamma_w \sum_{\tau=0}^k \|w_{k-\tau}\| \theta_z^\tau + \gamma_\varepsilon \sum_{\tau=0}^k \|\varepsilon_{y,k-\tau}\| \theta_z^\tau + \gamma_d \sum_{\tau=0}^k \|d_{k-\tau}\| \theta_z^\tau$$

$$\text{where } \delta = \max\{\bar{\varepsilon}_x^o, \bar{\varepsilon}_y^o, \bar{\Delta}_z^o, \bar{\Delta}_y^o, \bar{r}\}.$$

Proof. This proof is based on the proof of Theorem 2 in Wolff et al. (2024). For notational simplicity, we denote $\bar{\lambda}_\alpha = \lambda_\alpha(\bar{\varepsilon}_x^o + \bar{\varepsilon}_y^o + \bar{\Delta}_z^o + \bar{\Delta}_y^o)$.

(I) Lower and upper bounds for optimal cost V_k^*

A lower bound for optimal cost V_k^* has the following form:

$$\begin{aligned} (\eta_N V_k^*)^{\frac{1}{2}} &\geq \lambda_z \underline{p} \|\hat{z}_{k-N|k} - \bar{z}_{k-N}\| + \bar{\lambda}_\alpha \|\alpha_k^*\| \quad (19) \\ &\quad + \underline{q} \sum_{j=k-N}^k \|\pi_{j|k}^{z,*}\| + \sum_{j=k-N}^k \underline{r} \|\pi_{j|k}^{y,*}\| \end{aligned}$$

where \underline{p} , \underline{q} , and \underline{r} are the smallest eigenvalues of matrices P , Q , and R , respectively; $\eta_k = \lambda_z \underline{p} + \underline{q}(k+1) + \underline{r}(k+1) + \bar{\lambda}_\alpha$. Then, we leverage the trajectory of nominal system to construct a feasible solution for the proposed MHE (16), which provides an upper bound for optimal cost V_k^* . Based on condition (i) in Theorem 1, we select α_k as

$$\alpha_k = \begin{bmatrix} \mathcal{H}_N(u_{[0,T-1]}^o) \\ \mathcal{H}_N(v_{[0,T-1]}^o) \\ \mathcal{H}_1(z_{[0,T-N]}^o) \end{bmatrix}^\dagger \begin{bmatrix} u_{[k-N,k-1]} \\ v_{[k-N,k-1]} \\ z_{k-N} \end{bmatrix} \quad (20)$$

α_k satisfies:

$$\begin{bmatrix} \mathcal{H}_N(u_{[0,T-1]}^o) \\ \mathcal{H}_N(v_{[0,T-1]}^o) \\ \mathcal{H}_{N+1}(y_{[0,T]}^o) \\ \mathcal{H}_{N+1}(z_{[0,T]}^o) \end{bmatrix} \alpha_k = \begin{bmatrix} u_{[k-N,k-1]} \\ v_{[k-N,k-1]} \\ \tilde{y}'_{[k-N,k]} - \varepsilon_{y,[k-N,k]} \\ z_{[k-N,k]} \end{bmatrix}$$

where $\varepsilon_{y,[k-N,k]}$ is the actual online measurement noise from time instant $k-N$ to k . To satisfy (16a), we select

$$\pi_{[k-N,k]}^z = \mathcal{H}_{N+1}(\Delta z_{[0,T]}^o) \alpha_k + \mathcal{H}_{N+1}(\varepsilon_{z,[0,T]}^o) \alpha_k \quad (21a)$$

$$\begin{aligned} \pi_{[k-N,k]}^y &= \varepsilon_{y,[k-N,k]} + \Delta y_{[k-N,k]} - \mathcal{H}_{N+1}(\Delta y_{[0,T]}^o) \alpha_k \\ &\quad - \mathcal{H}_{N+1}(\varepsilon_{y,[0,T]}^o) \alpha_k \end{aligned} \quad (21b)$$

where $\varepsilon_{z,j}^o = \psi_\theta(x_j^o + \varepsilon_{x,j}^o) - \psi_\theta(x_j^o)$, $j \in \mathbb{N}_{[0,T]}$. An upper bound for V_k^* is established as follows:

$$\begin{aligned} (\eta_N V_k^*)^{\frac{1}{2}} &\leq \sqrt{\eta_N \lambda_z \bar{p}} \|z_{k-N} - \bar{z}_{k-N}\| + \sqrt{\eta_N \bar{\lambda}_\alpha} \|\alpha_k\| \\ &\quad + \sqrt{\eta_N \bar{q}} \sum_{j=k-N}^k \|\pi_j^z\| + \sqrt{\eta_N \bar{r}} \sum_{j=k-N}^k \|\pi_j^y\| \end{aligned} \quad (22)$$

where \bar{p} , \bar{q} , and \bar{r} are largest eigenvalues of matrices P , Q , and R , respectively. When $k < N$, the lower and upper bounds for the optimal cost V_k^* can be derived by replacing N with k in (19) and (22).

(II) Boundedness of estimation error $\|z_k - \hat{z}_{k|k}^*\|$

To establish an upper bound on the estimation error, we consider two trajectories of (15): 1) the nominal trajectory generated using α_k as defined in (20); 2) the estimated trajectory obtained using α_k^* . Specifically, given the initial condition z_{k-N} , the input sequence \mathbf{u} , and the scheduling parameter \mathbf{p} , the nominal state at time instant k is denoted as $z_k = z(N; z_{k-N}, \mathbf{0})$. The estimated state trajectory is initialized from \bar{z}_{k-N} , evolves under the same \mathbf{u} and \mathbf{p} , but is affected by the modeling residuals \mathbf{w} and \mathbf{d} . The estimated state at time instant k is denoted as $\hat{z}_k = z(N; \bar{z}_{k-N}, \mathbf{w})$. We select \bar{z}_{k-N} as follows:

$$\begin{aligned} \bar{z}_{k-N} &= \hat{z}_{k-N|k}^* + \pi_{k-N|k}^{z,*} - \mathcal{H}_1(\Delta z_{[0,T-N]}^o) \alpha_k^* \\ &\quad - \mathcal{H}_1(\varepsilon_{z,[0,T-N]}^o) \alpha_k^* \end{aligned} \quad (23)$$

Then, the state \hat{z}_k can be obtained as follows:

$$\hat{z}_k = \hat{z}_{k|k}^* + \pi_{k|k}^{z,*} - \mathcal{H}_1(\Delta z_{[N,T]}^o) \alpha_k^* - \mathcal{H}_1(\varepsilon_{z,[N,T]}^o) \alpha_k^* + \Delta z_k$$

It follows that

$$\begin{aligned} \|z_k - \hat{z}_{k|k}^*\| &\leq \|z_k - \hat{z}_k\| + \|\pi_{k|k}^{z,*}\| + \|\mathcal{H}_1(\Delta z_{[N,T]}^o) \alpha_k^*\| \\ &\quad + \|\mathcal{H}_1(\varepsilon_{z,[N,T]}^o) \alpha_k^*\| + \|\Delta z_k\| \end{aligned} \quad (24)$$

According to (17) and (23), it holds that

$$\begin{aligned} \|z_k - \hat{z}_k\| &\leq c_z \|z_{k-N} - \hat{z}_{k-N|k}^*\| \xi^N + c_z \|\pi_{k-N|k}^{z,*}\| \xi^N \\ &\quad + c_z \|\mathcal{H}_1(\Delta z_{[0,T-N]}^o) \alpha_k^*\| \xi^N + c_z \|\mathcal{H}_1(\varepsilon_{z,[0,T-N]}^o) \alpha_k^*\| \xi^N \\ &\quad + c_h \sum_{\tau=0}^{N-1} \|h(z(\tau; z_{k-N}, \mathbf{0}), \mathbf{0}) - h(z(\tau; \hat{z}_{k-N}, \mathbf{w}), \mathbf{d})\| \\ &\quad \times \xi^{N-\tau-1} + c_w \sum_{\tau=0}^{N-1} \|w_{k-N+\tau}\| \xi^{N-\tau-1} \end{aligned} \quad (25)$$

Then, we establish upper bounds for each term on the right-hand side of (25). It follows from $0 < \xi < 1$ that $c_z \|\pi_{k-N|k}^{z,*}\| \xi^N + \|\pi_{k|k}^{z,*}\| \leq (c_z + 1) \|\pi_{k-N|k}^{z,*}\|$. Note that $h(z(\tau; z_{k-N}, \mathbf{0}), \mathbf{0}) = \tilde{y}_{k-N+\tau} - \Delta y_{k-N+\tau} - \varepsilon_{y,k-N+\tau}$ and $h(z(\tau; \hat{z}_{k-N}, \mathbf{w}), \mathbf{d}) = \mathcal{H}_1(y_{[\tau,T-N+\tau]}^o) \alpha_k^* + \Delta y_{k-N+\tau} = \tilde{y}_{k-N+\tau} - \pi_{k-N+\tau|k}^{y,*} - \mathcal{H}_1(\varepsilon_{y,[\tau,T-N+\tau]}^o) \alpha_k^* - \mathcal{H}_1(\Delta y_{[\tau,T-N+\tau]}^o) \alpha_k^* + \Delta y_{k-N+\tau}$ hold for $\tau \in \mathbb{N}_{[0,N]}$ with $\Delta y_{k-N+\tau} = CD \Delta z_{k-N+\tau} + d_{k-N+\tau}$. One can obtain that

$$\begin{aligned} &\|h(z(\tau; z_{k-N}, \mathbf{0}), \mathbf{0}) - h(z(\tau; \hat{z}_{k-N}, \mathbf{w}), \mathbf{d})\| \\ &\leq 2 \|\Delta y_{k-N+\tau}\| + \|\varepsilon_{y,k-N+\tau}\| + \|\pi_{k-N+\tau|k}^{y,*}\| \\ &\quad + \|\mathcal{H}_1(\varepsilon_{y,[\tau,T-N+\tau]}^o) \alpha_k^*\| + \|\mathcal{H}_1(\Delta y_{[\tau,T-N+\tau]}^o) \alpha_k^*\| \end{aligned} \quad (26)$$

Finally, we establish upper bounds for the terms associated with α_k^* . Following Wolff et al. (2024), we have

$$\|\mathcal{H}_1(\varepsilon_{y,[\tau,T-N+\tau]}^o)\| \leq \sqrt{n_y(T-N+1)} \bar{\varepsilon}_y^o \quad (27)$$

We can obtain upper bounds for $\|\mathcal{H}_1(\Delta y_{[\tau,T-N+\tau]}^o)\|$ and $\|\mathcal{H}_1(\Delta z_{[\tau,T-N+\tau]}^o)\|$ in a similar way. By leveraging Lipschitz continuity of the lifting function ψ_θ from Assumption 4, it follows that $\|\varepsilon_{z,j}^o\| = \|\psi_\theta(x_j^o + \varepsilon_{x,j}^o) - \psi_\theta(x_j^o)\| \leq L_\psi \bar{\varepsilon}_x^o$. Then, we have that

$$\|\mathcal{H}_1(\varepsilon_{z,[\tau,T-N+\tau]}^o)\| \leq \sqrt{n_z(T-N+1)} L_\psi \bar{\varepsilon}_x^o \quad (28)$$

Selecting $c_\alpha = \max\{(c_z + 1) \sqrt{n_z(T-N+1)} L_\psi, (c_z + 1) \sqrt{n_z(T-N+1)}, c_h N \sqrt{n_y(T-N+1)}\}$ and substituting (25)-(28) into (24) yield

$$\|z_k - \hat{z}_{k|k}^*\| \leq c_z \|z_{k-N} - \bar{z}_{k-N}\| \xi^N + c_z \|\hat{z}_{k-N|k}^* - \bar{z}_{k-N}\| \xi^N + (c_z + 1) \|\pi_{[k-N, k]|k}^{z,*}\| + \|\Delta z_k\| + \bar{c}_\alpha \|\alpha_k^*\| \quad (29)$$

$$+ c_h \sum_{\tau=0}^{N-1} \|\pi_{k-N+\tau|k}^{y,*}\| + c_h \sum_{\tau=0}^{N-1} (\|\varepsilon_{y, k-N+\tau}\| + 2\Delta y_{k-N+\tau}\|) \xi^{N-\tau-1} + c_w \sum_{\tau=0}^{N-1} \|w_{k-N+\tau}\| \xi^{N-\tau-1}$$

where $\bar{c}_\alpha = c_\alpha (\bar{\varepsilon}_x^o + \bar{\varepsilon}_y^o + \bar{\Delta}_y^o + \bar{\Delta}_z^o)$. When $k < N$, (29) holds by replacing N with k . Denote $k = \tilde{k} + jN$ with $\tilde{k} \in \mathbb{N}_{[0, N-1]}$ and $j \in \mathbb{N}$.

(II.a) Case I: $k \geq N$. Select $\epsilon \in (0, 1)$ and an estimation horizon N such that $c_z \xi^N \leq \epsilon$. The smallest value of N satisfying this condition is denoted by N_0 . Select λ_α, P, Q , and R such that $\epsilon \leq \lambda_z \underline{p}$, $c_z + 1 \leq \underline{q}$, $c_h \leq \underline{r}$, and $c_\alpha \leq \lambda_\alpha$. Considering (19) and (22), we derive from (29) that

$$\begin{aligned} & \|z_{\tilde{k}+N} - \hat{z}_{\tilde{k}+N|\tilde{k}+N}^*\| \\ & \leq (\epsilon + \sqrt{\eta_N \lambda_z \bar{p}}) \|z_{\tilde{k}} - \bar{z}_{\tilde{k}}\| + \sqrt{\eta_N \bar{\lambda}_\alpha} \|\alpha_{\tilde{k}+N}\| \\ & + \sqrt{\eta_N \bar{q}} \sum_{\tau=0}^N \|\pi_{\tilde{k}+\tau}^z\| + \sqrt{\eta_N \bar{r}} \sum_{\tau=0}^N \|\pi_{\tilde{k}+\tau}^y\| + \|\Delta z_{\tilde{k}+N}\| \\ & + \sum_{\tau=0}^{N-1} (c_h (2\|\Delta y_{\tilde{k}+\tau}\| + \|\varepsilon_{y, \tilde{k}+\tau}\|) + c_w \|w_{\tilde{k}+\tau}\|) \xi^{N-\tau-1} \end{aligned} \quad (30)$$

From (21) and the derivation of (27), it holds that

$$\begin{aligned} \|\pi_{\tilde{k}+\tau}^z\| & \leq \sqrt{n_z(T-N+1)} (L_\psi \bar{\varepsilon}_x^o + \bar{\Delta}_z^o) \|\alpha_{\tilde{k}+N}\| \\ \|\pi_{\tilde{k}+\tau}^y\| & \leq \|\varepsilon_{y, \tilde{k}+\tau}\| + \|\Delta y_{\tilde{k}+\tau}\| \\ & + \sqrt{n_y(T-N+1)} (\bar{\varepsilon}_y^o + \bar{\Delta}_y^o) \|\alpha_{\tilde{k}+N}\| \end{aligned} \quad (31)$$

Moreover, we have $\|\Delta z_{\tilde{k}+\tau}\| \leq \omega_A \sum_{i=0}^{\tau-1} \|w_{\tilde{k}+i}\|$ and $\|\Delta y_{\tilde{k}+\tau}\| \leq \|C\| \|D\| \|\Delta z_{\tilde{k}+\tau}\| + \|d_{\tilde{k}+\tau}\|$ with $\omega_A = \max\{1, \|A\|^{N-1}\}$. Given that $u_k \in \mathcal{U}$ and $x_k \in \mathcal{X}$, the continuity of ψ_θ and λ_σ implies that $z_k = \psi_\theta(x_k)$ and $p_k = \lambda_\sigma(z_k, u_k)$ are contained in compact sets. Therefore, there exist \bar{u} , \bar{z} , and \bar{p} , such that $\|u_k\| \leq \bar{u}$, $\|z_k\| \leq \bar{z}$, and $\|p_k\| \leq \bar{p}$ hold for all $k \in \mathbb{N}$. It follows that $\|v_k\| \leq \bar{u} \bar{p}$. Following Wolff et al. (2024), there exists an upper bound $\bar{\alpha}$ such that $\|\alpha_k\| \leq \bar{\alpha}$. By (31), (30) can be reformulated as follows:

$$\begin{aligned} & \|z_{\tilde{k}+N} - \hat{z}_{\tilde{k}+N|\tilde{k}+N}^*\| \leq \omega_z \|z_{\tilde{k}} - \bar{z}_{\tilde{k}}\| + \omega(\varpi) \\ & + \sum_{\tau=0}^N (\omega_w \|w_{\tilde{k}+\tau}\| + \omega_\varepsilon \|\varepsilon_{y, \tilde{k}+\tau}\| + \omega_d \|d_{\tilde{k}+\tau}\|) \xi^{N-\tau-1} \end{aligned} \quad (32)$$

where $\omega_z = \epsilon + \sqrt{\eta_N \lambda_z \bar{p}}$, $\omega_\varepsilon = \sqrt{\eta_N \bar{r}} \xi^{1-N} + c_h$, $\omega_d = \sqrt{\eta_N \bar{q}} \xi^{1-N} + 2c_h$, $\omega_w = c_w + \omega_d \|C\| \|D\| \omega_A (N+1) + \omega_A \xi^{1-N}$, $\varpi = \max\{\bar{\varepsilon}_x^o, \bar{\varepsilon}_y^o, \bar{\Delta}_z^o, \bar{\Delta}_y^o\}$, and $\omega(\varpi) = ((\frac{2c_\alpha}{c_z+1}) \sqrt{\eta_N \bar{q}} + \frac{2c_\alpha(N+1)}{c_h N} \sqrt{\eta_N \bar{r}}) \varpi + \sqrt{\eta_N \bar{\lambda}_\alpha} \bar{\alpha}$.

Since $\omega_z \leq \lambda_z \underline{p} + \sqrt{\eta_N \lambda_z \bar{p}}$, the condition $\omega_z < 1$ can be satisfied by tuning λ_z . For $j > 1$, by jointly considering the fact that $\bar{z}_\tau = \hat{z}_{\tau|\tau}^*$ and (32), it is further obtained that

$$\begin{aligned} & \|z_{\tilde{k}+jN} - \hat{z}_{\tilde{k}+jN|\tilde{k}+jN}^*\| \leq \|z_{\tilde{k}} - \bar{z}_{\tilde{k}}\| \omega_z^j + \frac{1}{1-\omega_z} \omega(\varpi) \\ & + \sum_{i=0}^{j-1} \omega_z^i \sum_{\tau=0}^N (\omega_w \|w_{\tilde{k}+(j-i)N-\tau}\| + \omega_\varepsilon \|\varepsilon_{y, \tilde{k}+(j-i)N-\tau}\|) \end{aligned}$$

$$+ \omega_d \|d_{\tilde{k}+(j-i)N-\tau}\| \xi^{\tau-1} \quad (33)$$

(II.b) Case II: $k < N$. According to the lower and upper bounds established in Wolff et al. (2024), one has

$$\|\hat{z}_{0|k}^* - \bar{z}_0\| \leq \sigma \|z_0 - \bar{z}_0\| + \sum_{\tau=0}^k (\sigma_z \|\pi_\tau^z\| + \sigma_y \|\pi_\tau^y\|) + \sigma_\alpha \|\alpha_k\|$$

where $\sigma = \sqrt{\bar{p}/\underline{p}}$, $\sigma_z = \sqrt{\bar{q}/\lambda_z \underline{p}}$, $\sigma_y = \sqrt{\bar{r}/\lambda_z \underline{p}}$, and $\sigma_\alpha = \sqrt{\bar{\lambda}_\alpha/\lambda_z \underline{p}}$. Since $c_z \xi^N \leq \epsilon \leq \lambda_z \underline{p}$, applying the same procedure to derive (32) yields

$$\|z_k - \hat{z}_{k|k}^*\| \leq \rho_z \|z_0 - \bar{z}_0\| + \rho(\varpi) \quad (34)$$

$$+ \sum_{\tau=0}^k (\rho_w \|w_\tau\| + \rho_\varepsilon \|\varepsilon_{y, \tau}\| + \rho_d \|d_\tau\|) \xi^{k-\tau-1}$$

where $\tilde{c}_z = c_z (1 - \xi^N)$, $\rho_z = \epsilon + \tilde{c}_z \sigma + \sqrt{\eta_N \lambda_z \bar{p}}$, $\rho_\varepsilon = (\sqrt{\eta_N \bar{r}} + \tilde{c}_z \sigma_y) \xi^{1-N} + c_h$, $\rho_d = (\sqrt{\eta_N \bar{q}} + \tilde{c}_z \sigma_z) \xi^{1-N} + 2c_h$, and $\rho_w = \omega_w$, $\rho(\varpi) = (\tilde{c}_z \sigma_\alpha + (\frac{2c_\alpha(\sqrt{\eta_N \bar{q}} + \tilde{c}_z \sigma_y)}{(c_z+1)}) \varpi + \sqrt{\eta_N \bar{\lambda}_\alpha}) \bar{\alpha}$. Select $\theta_z = \omega_z^{\frac{1}{2N}}$, which satisfies $\omega_z^j \leq \theta_z^{\tilde{k}+jN}$ for $\tilde{k} \in [0, N]$, $j \in \mathbb{N}_{[1, \infty)}$. It follows that

$$\sum_{\tau=0}^{\tilde{k}} \|w_{\tilde{k}-\tau}\| \omega_z^j + \sum_{i=0}^{j-1} \sum_{\tau=0}^N \|w_{\tilde{k}+(j-i)N-\tau}\| \omega_z^i \leq \tilde{\rho} \sum_{\tau=0}^k \|w_{k-\tau}\| \theta_z^\tau \quad (35)$$

where $\tilde{\rho} = \max\{2, \theta_z^{1-N}\}$. By substituting (34) into (33) and applying the procedure of (35) to the terms involving $\varepsilon_{y, k}$ and d_k , we obtain

$$\begin{aligned} & \|z_k - \hat{z}_{k|k}^*\| \leq \rho_z \|z_0 - \bar{z}_0\| \theta_z^k + \theta(\varpi) \\ & + \sum_{\tau=0}^k (\gamma_w \|w_{k-\tau}\| + \gamma_\varepsilon \|\varepsilon_{y, k-\tau}\| + \gamma_d \|d_{k-\tau}\|) \theta_z^\tau \end{aligned}$$

where $\gamma_w = \rho_w \xi^{-1} \tilde{\rho}$, $\gamma_\varepsilon = \rho_\varepsilon \xi^{-1} \tilde{\rho}$, $\gamma_d = \rho_d \xi^{-1} \tilde{\rho}$, and $\theta(\varpi) = \rho(\varpi) + \frac{\omega(\varpi)}{1-\omega_z}$. By (15c), we further derive that

$$\begin{aligned} & \|x_k - \hat{x}_{k|k}^*\| \leq \|D\| (\rho_z L_\psi \|x_0 - \bar{x}_0\| \theta_z^k + \sum_{\tau=0}^k (\gamma_w \|w_{k-\tau}\| \\ & + \gamma_\varepsilon \|\varepsilon_{y, k-\tau}\| + \gamma_d \|d_{k-\tau}\|) \theta_z^\tau + \theta(\varpi)) + \bar{r} \end{aligned}$$

5. APPLICATIONS TO MEMBRANE BIOREACTOR

5.1 Process description

We consider a membrane bioreactor used for wastewater treatment, with a schematic illustration provided in Fig. 2 (Maere et al. (2011)). This plant comprises two anoxic tanks and three aerobic tanks, with the final aerobic tank being equipped with a membrane module for filtration. In the anoxic tanks, predenitrification occurs to convert nitrate into gaseous nitrogen. In the aerobic tanks, the ammonium is oxidized into nitrite through nitrification. The membrane bioreactor integrates membrane modules within the fifth tank for filtration (Maere et al. (2011)).

Two streams are fed into the first anoxic tank: 1) the influent wastewater at concentration Z_f and flow rate Q_f ; 2) a recycle stream from the outlet of the second aerobic tank at concentration Z_{r2} and flow rate Q_{r2} .

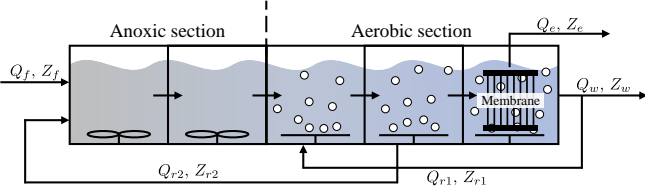


Fig. 2. A schematic of the membrane bioreactor for wastewater treatment Maere et al. (2011).

The outlet of the membrane bioreactor process consists of three parts: 1) the permeate, which contains purified water through membrane filtration, continuously withdrawn at concentration Z_e and flow rate Q_e ; 2) a sludge recycle stream, returned from the third aerobic tank to the first aerobic tank with concentration Z_{r1} and flow rate Q_{r1} ; 3) the waste sludge stream, discharged at concentration Z_w and flow rate Q_w (Maere et al. (2011)).

This process comprises eight biological reactions, and it involves thirteen major substances. The concentrations of these substances in five biological reactors constitute the 65 state variables of this process. The definitions of these state variables and a detailed description of the membrane bioreactor process can be found in Maere et al. (2011). To monitor the process, eight sensors are assumed to be installed in each biological tank, which can be found in Table 3 in Li et al. (2023). The control inputs of the membrane bioreactor process comprise the airflow rate $Q_{a,i}$, $i \in \mathbb{N}_{[1,3]}$, in three aerobic tanks and the internal recycle flow rate Q_{r2} . Additionally, this system is influenced by uncontrollable inputs, including inlet flow rate Q_f and the concentration Z_f of thirteen inlet substances. The corresponding influent data profiles are obtained from the International Water Association website¹ (Alex et al. (2008)). The sampling period of this process is selected as 15 min.

5.2 Simulation setting

The dataset $\{u_k, \tilde{x}_k, \tilde{y}_k\}_1^T$ of length $T = 53760$ is generated through open-loop simulations of the first-principles model in Guo et al. (2020). This dataset is partitioned into a training set with 43008 samples and a validation set with 10752 samples. Additionally, another dataset $\{u_k, \tilde{x}_k, \tilde{y}_k\}_1^T$ of length $T = 1344$ for an operating period of 14 days is generated for testing. The initial condition for generating the datasets is selected as one steady-state open-loop point of the membrane bioreactor process, as presented in Maere et al. (2011). The control inputs are randomly generated following a uniform distribution between u_{\min} and u_{\max} , with $u_{\min} = [4000 \text{ Nm}^3/\text{h}, 2000 \text{ Nm}^3/\text{h}, 5000 \text{ Nm}^3/\text{h}, 0 \text{ m}^3/\text{day}]^\top$ and $u_{\max} = [4500 \text{ Nm}^3/\text{h}, 2500 \text{ Nm}^3/\text{h}, 38012 \text{ Nm}^3/\text{h}, 160900 \text{ m}^3/\text{day}]^\top$. Each sampled control input is kept constant for 40 sampling periods. Additive unknown noise is generated following a Gaussian distribution of zero mean and standard deviation of $0.01 \times u_{\max}$ and is added to the control input. Note that the five state variables (i.e., S_I in each tank) remain invariant throughout the entire simulation; these states are excluded from the datasets.

¹ <http://www.benchmarkwwtp.org>

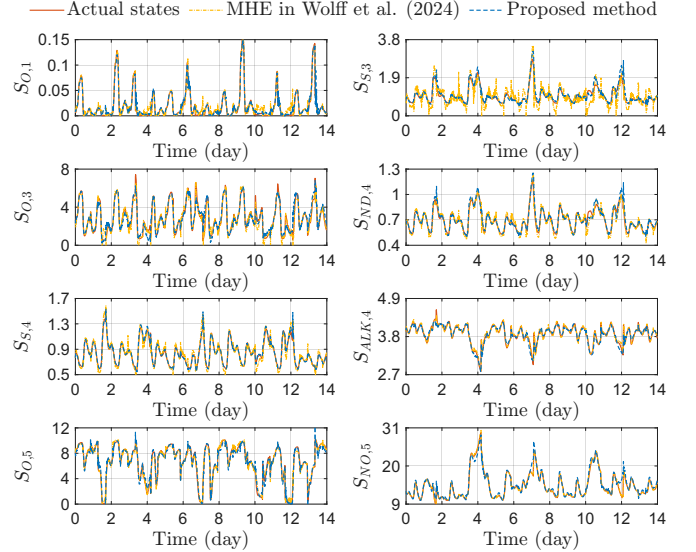


Fig. 3. Trajectories of selected actual states and state estimates provided by the proposed MHE in (16) and MHE in Wolff et al. (2024) under dry weather.

To implement the proposed learning-based data-enabled MHE approach, the scheduling parameter of (5) is considered to be $p \in \mathbb{R}$. ψ_θ and λ_σ are trained as two DNNs (Rumelhart et al. (1986)) to approximate the state lifting function and the scheduling mapping. ψ_θ is structured with two hidden layers comprising 128 and 256 neurons, respectively, while λ_σ consists of three hidden layers with 128, 256, and 256 neurons, respectively. For both networks, the rectified linear unit (ReLU) (Goodfellow et al. (2016)) is utilized as the activation function after the input and hidden layers. The training process is performed over 400 epochs with a batch size of 256 using Adam optimizer (Kingma and Ba. (2014)) with a learning rate of 10^{-4} .

The dataset for the implementation of the proposed data-enabled MHE is constructed in the same way as the one used for neural network training. During offline stage, the dataset $\{u_k, \tilde{x}_k, \tilde{y}_k\}_1^T$ of length $T = 3000$ is generated. Additive measurement noise, which is sampled from the Gaussian distributions with zero mean and standard deviation of $10^{-4} \times x_0$ and $10^{-4} \times y_0$, is introduced to the state and measured output, respectively. Subsequently, the trained neural networks ψ_θ and λ_σ are employed to generate the lifted state $\{\tilde{z}_k\}_1^T$ and scheduling parameter $\{p_k\}_1^T$. The resulting dataset $\{u_k, \tilde{z}_k, \tilde{y}_k, p_k\}_1^T$ is utilized to construct the Hankel matrix. For online implementation, the output measurement noise is generated in the same way as in the offline stage. The initial guess \bar{x}_0 is selected as $1.05 \times x_0$. The parameters of the proposed MHE scheme are adopted from Wolff et al. (2024). We select $\bar{\Delta}_z^o = 0.003$, $\bar{\Delta}_y^o = 0.003$, and estimation horizon $N = 4$.

5.3 Estimation results

We consider the dry weather condition, and the proposed method provides accurate estimates of the states of the membrane bioreactor process. The estimation results for selected state variables obtained using the proposed design in (16) are presented in Fig. 3. We also evaluate the estimation performance of the data-enabled MHE method

in Wolff et al. (2024), using identical parameters for fair comparison. As shown in Fig. 3, the proposed method outperforms the MHE approach in Wolff et al. (2024) for the nonlinear membrane bioreactor process in terms of estimation accuracy.

6. CONCLUSION

We proposed a learning-based data-enabled MHE approach for nonlinear systems. This approach leverages an LPV Koopman representation of the underlying nonlinear system and employs two neural networks to construct the trajectories of this Koopman representation directly from system data. A data-enabled MHE was then formulated, which enables the reconstruction of the original nonlinear system states from the state estimates of the Koopman surrogate. The proposed approach does not require explicit model identification and formulates a convex optimization-based MHE design for nonlinear systems. The stability of the proposed method was analyzed. The proposed method provides more accurate estimates than the benchmark data-enabled MHE for a membrane-based biological water treatment process.

REFERENCES

F. Allgöwer and A. Zheng. Nonlinear model predictive control. *Birkhäuser*, 2012.

J. H. Lee and J. M. Lee. Progress and challenges in control of chemical processes. *Annual Review of Chemical and Biomolecular Engineering*, 5(1):383–404, 2014.

W. Bourgeois, J. E. Burgess, and R. M. Stuetz. On-line monitoring of wastewater quality: a review. *Journal of Chemical Technology & Biotechnology*, 76(4):337–348, 2001.

M. S. Turan and G. Ferrari-Trecate. Data-driven unknown-input observers and state estimation. *IEEE Control Systems Letters*, 6:1424–1429, 2021.

K. K. Kottakki, S. Bhartiya, and M. Bhushan. State estimation of nonlinear dynamical systems using nonlinear update based unscented Gaussian sum filter. *Journal of Process Control*, 24(9):1425–1443, 2014.

X. Shao, B. Huang, and J. M. Lee. Constrained Bayesian state estimation—A comparative study and a new particle filter based approach. *Journal of Process Control*, 20(2):143–157, 2010.

C. V. Rao, J. B. Rawlings, and D. Q. Mayne. Constrained state estimation for nonlinear discrete-time systems: Stability and moving horizon approximations. *IEEE Transactions on Automatic Control*, 48(2):246–258, 2003.

C. V. Rao, J. B. Rawlings, and J. H. Lee. Constrained linear state estimation—a moving horizon approach. *Automatica*, 37(10):1619–1628, 2001.

X. Yin, Y. Qin, J. Liu, and B. Huang. Data-driven moving horizon state estimation of nonlinear processes using Koopman operator. *Chemical Engineering Research and Design*, 200:481–492, 2023.

J. C. Willems, P. Rapisarda, I. Markovsky, and B. L. De Moor. A note on persistency of excitation. *Systems & Control Letters*, 54(4):325–329, 2005.

J. Berberich and F. Allgöwer. A trajectory-based framework for data-driven system analysis and control. *European Control Conference*, 1365–1370, 2020.

M. M. Morato and M. S. Felix. Data science and model predictive control: A survey of recent advances on data-driven MPC algorithms. *Journal of Process Control*, 144:103327, 2024.

R. Adachi and Y. Wakasa. Dual system representation and prediction method for data-driven estimation. *Annual Conference of the Society of Instrument and Control Engineers of Japan*, 1245–1250, 2021.

T. M. Wolff, V. G. Lopez, and M. A. Müller. Robust data-driven moving horizon estimation for linear discrete-time systems. *IEEE Transactions on Automatic Control*, 69(8):5598–5604, 2024.

M. C. Nicoletti, L. C. Jain, and R. C. Giordano. Computational intelligence techniques as tools for bioprocess modelling, optimization, supervision and control. *Berlin/Heidelberg: Springer*, 2009.

Z. Xiong, Z. Yuan, K. Miao, H. Wang, J. Cortés, and A. Papachristodoulou. Data-enabled predictive control for nonlinear systems based on a Koopman bilinear realization. *arXiv preprint arXiv:2505.03346*, 2025.

B. O. Koopman. Hamiltonian systems and transformation in Hilbert space. *Proceedings of the National Academy of Sciences*, 17(5):315–318, 1931.

L. C. Iacob, R. Tóth, and M. Schoukens. Koopman form of nonlinear systems with inputs. *Automatica*, 162:111525, 2024.

R. Tóth, H. S. Abbas, and H. Werner. On the state-space realization of LPV input-output models: Practical approaches. *IEEE Transactions on Control Systems Technology*, 20(1):139–153, 2011.

L. C. Iacob, M. Szécsi, G. I. Beintema, M. Schoukens, and R. Tóth. Learning Koopman models from data under general noise conditions. *arXiv preprint arXiv:2507.09646*, 2025.

X. Zhang, W. Pan, R. Scattolini, S. Yu, and X. Xu. Robust tube-based model predictive control with Koopman operators. *Automatica*, 137:110114, 2022.

H. J. Van Waarde, C. De Persis, M. K. Camlibel, and P. Tesi. Willems' fundamental lemma for state-space systems and its extension to multiple datasets. *IEEE Control Systems Letters*, 4(3):602–607, 2020.

D. E. Rumelhart, G. E. Hinton, and R. J. Williams. Learning representations by back-propagating errors. *Nature*, 323(6088):533–536, 1986.

A. Alessandri. Robust moving horizon estimation for nonlinear systems: From perfect to imperfect optimization. *Automatica*, 175:112187, 2025.

T. Maere, B. Verrecht, S. Moerenhout, S. Judd, and I. Nopens. BSM-MBR: a benchmark simulation model to compare control and operational strategies for membrane bioreactors. *Water Research*, 45(6):2181–2190, 2011.

X. Guo, P. Hong, and T. M. Laleg-Kirati. Nonlinear model predictive control design for BSM-MBR: benchmark of membrane bioreactor. *IFAC-PapersOnLine*, 53(2):16524–16530, 2020.

X. Li, A.W.-K. Law, and X. Yin. Partition-based distributed extended Kalman filter for large-scale nonlinear processes with application to chemical and wastewater treatment processes. *AIChE Journal*, 69(12):e18229, 2023.

J. Alex, L. Benedetti, J. Copp, K.V. Gernaey, U. Jeppsson, I. Nopens, M.-N Pons, L. Rieger, C. Rosen, J. P. Steyer,

P. Vanrolleghem, and S. Winkler. Benchmark simulation model no. 1 (BSM1). *Technical Report*, 2008.

D. P. Kingma and J. Ba. Adam: A method for stochastic optimization. *International Conference on Learning Representations*, 2014.

I. Goodfellow, Y. Bengio, A. Courville, and Y. Bengio. Deep learning. *MIT Press*, 2016.